Mon. Not. R. Astron. Soc. **385,** 381–390 (2008) doi:10.1111/j.1365-2966.2007.12832.x

The early-type semidetached binary system V716 Centaurus

H. Bakış,★ V. Bakış, O. Demircan and Z. Eker
Çanakkale Onsekiz Mart University Observatory, Terzioğlu Campus, TR-17040 Çanakkale, Turkey

Accepted 2007 December 7. Received 2007 December 4; in original form 2007 August 29

Downloaded from https://academic.oup.com/mnras/article/385/1/381/1032418 by Akdeniz University user on 20 September 2021

ABSTRACT

New high-resolution spectra of V716 Cen revealed for the first time lines of the secondary component and its radial velocities. The simultaneous solution of the new radial velocity curves and the *Hipparcos* light curve yield the reliable absolute dimensions of this semidetached system. The masses for the primary and secondary are $M_1 = 5.68 \pm 0.07\,\mathrm{M}_\odot$ and $M_2 = 2.39 \pm 0.05\,\mathrm{M}_\odot$, respectively, and the radii are $R_1 = 4.08 \pm 0.07\,\mathrm{R}_\odot$ and $R_2 = 3.36 \pm 0.02\,\mathrm{R}_\odot$. We derive also effective temperatures of $T_{\mathrm{eff1}} = 15\,500 \pm 50$ K and $T_{\mathrm{eff2}} = 9000 \pm 80$ K, and equatorial rotational velocities of $v_{\mathrm{rot}} \sin i = 137 \pm 2$ km s^{-1} and $v_{\mathrm{rot}} \sin i = 116 \pm 7$ km s^{-1}. These rotational velocities imply that the components rotate synchronously. The distance to the system is $d = 339 \pm 8$ pc, in good agreement with the less accurate *Hipparcos* distance (337 ± 72 pc). The primary is underluminous and the secondary overluminous compared to normal main-sequence stars of the same mass. This implies that the secondary component of the semidetached system is in slow mass transferring stage after mass ratio reversal, although the Hα-line profiles do not show clear evidence for this.

Key words: binaries: eclipsing – stars: early-type – stars: emission-line, Be – stars: fundamental parameters – stars: individual: V716 Cen.

1 INTRODUCTION

V716 Centaurus (HD124195, B5Ve) is a bright ($V = 6.052$ mag), southern eclipsing binary with an orbital period of ∼1.49 d. After its first light curve was published by Schöffel & Köhler (1965), Chambliss (1969) discussed out-of-eclipse variations. But Wesselius (1981), who studied V716 Cen optically including ultraviolet data of the Dutch satellite *ANS*, has not confirmed such out-of-eclipse variations. Several studies (e.g. Cousins & Stoy 1962; Johnson et al. 1966; Fitzgerald 1970; Deutschman, Davis & Schild 1976; Wesselius et al. 1980; Hauck & Mermilliod 1998) discussed the brightness and the colours of the system.

Despite its brightness and short orbital period, V716 Cen is not yet well studied: no complete radial velocity (RV) curve is published, the photometry relies on the *Hipparcos* satellite (ESA 1997) and no colour information is available in the eclipses.

Early spectroscopic observations of V716 Cen were discussed by Popper (1966) who saw the system as a single-lined one, but did not give an orbital solution nor RV data. Later, Hube (1970) published three RVs of V716 Cen (92, 95, 10 km s^{-1}). On the basis of the mean of these velocities (65.9 km s^{-1}) and being unaware of the previous studies, Bekenstein & Bowers (1974) included the system in a list of potential runaway stars. Hoogerwerf, de Bruijne & de Zeeuw (2001) studied the space velocity of V716 Cen and found the system's path crossing the Upper Centaurus–Lupus and the Cep OB6 associations. They have found a kinematic age smaller than the ages of both associations, and conclude that V716 Cen is not a member of either of these.

Harmanec (2001) included V716 Cen in his preliminary list of interacting binary stars with OBAe component. The primary motivation of this study is to investigate if V716 Cen contains a Be-type component; thus we have obtained high-resolution spectra, which are also useful to study the RV variations of the component stars. The present paper is designed in the following way. Spectroscopic observations and the reduction of high-resolution échelle spectra are described in Section 2. RV measurements and a spectroscopic orbital solution are made in Section 3. The simultaneous solution of light and RV curves is given in Section 4. Finally, we discuss the synchronization and the astrophysical parameters of the components, followed by an investigation of the circumstellar matter in the system and a discussion on the evolutionary status in Section 5.

2 SPECTROSCOPIC OBSERVATIONS AND DATA REDUCTION

The spectra of V716 Cen were taken using HERCULES (High Efficiency and Resolution Canterbury University Large Echelle Spectrograph). It is a fibre-fed échelle spectrograph attached to the 1-m McLellan telescope at the Mt John University Observatory (MJUO), near Lake Tekapo (∼43°59′ S, 174°27′ E). The spectrograph is mounted on a stable optical bench and enclosed within a vacuum vessel located in a thermally insulated room. Light from the Cassegrain focus can be fed to the spectrograph using a 20-m length of optical

★E-mail: bhicran@comu.edu.tr (HB)

© 2008 The Authors. Journal compilation © 2008 RAS

Table 1. Journal of spectroscopic observations. Date column refers to the local date of the start of night.

No.	Frame	HJD (−240 0000)	Date	UT	Exposure time (s)
1	w3966028s.fit	539 66.893 66	19.08.2006	09:27:23	868
2	w3967032s.fit	539 67.829 64	20.08.2006	07:55:18	1374
3	w3967044s.fit	539 67.923 87	20.08.2006	10:11:00	1759
4	w3967054s.fit	539 67.977 23	20.08.2006	11:27:52	1800
5	w3969017s.fit	539 69.828 73	22.08.2006	07:54:13	702
6	w3969023s.fit	539 69.867 52	22.08.2006	08:50:05	1099
7	w3969029s.fit	539 69.897 77	22.08.2006	09:33:39	901
8	w3971038s.fit	539 71.986 01	24.08.2006	11:40:56	936
9	w3971039s.fit	539 71.998 55	24.08.2006	11:59:00	1121
10	w3976074s.fit	539 76.953 99	29.08.2006	10:55:22	969
11	w3976075s.fit	539 76.967 30	29.08.2006	11:14:32	1095
12	w3977033s.fit	539 77.802 97	30.08.2006	07:17:59	487
13	w3977039s.fit	539 77.818 95	30.08.2006	07:41:00	498
14	w3977045s.fit	539 77.835 65	30.08.2006	08:05:03	499
15	w3977051s.fit	539 77.853 79	30.08.2006	08:31:10	709
16	w3977057s.fit	539 77.872 76	30.08.2006	08:53:55	548
17	w3977066s.fit	539 77.906 06	30.08.2006	09:41:35	585
18	w3977072s.fit	539 77.925 81	30.08.2006	10:14:54	563
19	w3977078s.fit	539 77.945 31	30.08.2006	10:42:58	606
20	w3986086s.fit	539 86.949 14	08.09.2006	10:49:25	950
21	w3988085s.fit	539 88.915 25	10.09.2006	10:00:50	567
22	w3988091s.fit	539 88.943 53	10.09.2006	10:41:33	690
23	w3988092s.fit	539 88.951 98	10.09.2006	10:53:43	666
24	w3989106s.fit	539 89.889 51	11.09.2006	09:23:51	588
25	w3989112s.fit	539 89.906 80	11.09.2006	09:48:45	593
26	w3991090s.fit	539 91.911 33	13.09.2006	09:55:29	530
27	w3995002s.fit	539 95.920 97	17.09.2006	10:09:44	706

fibre of selectable cross-section (Hearnshaw et al. 2002). The spectrograph is designed to provide continuous wavelength coverage from $\lambda = 380$–880 nm in over 80 échelle orders. Two resolving powers of $R = 41\,000$ and 70 000 are possible to obtain high-precision spectroscopic observations of a variety of objects over extended times. Choices of resolving power is made possible by selecting one of the three optical fibres with different sizes. Fibre 1, which is a 100-μm fibre with no slit giving a moderately high resolving power of 41 000, has been selected for the observations of this project. The angular size of the fibre core projected on to the sky ($\theta \sim 4.5$ arcsec) is not less then the median seeing at MJUO which was reported to be about 3.5 arcsec (Hearnshaw et al. 2002). Fibres 2 and 3 have a resolving power of $R = 70\,000$ but require good seeing conditions ($\theta \sim 2$ arcsec). A more detailed description of the spectrograph can be found in Hearnshaw et al. (2002) and Skuljan, Ramm & Hearnshaw (2004).

The 4000 × 4000 spectral instruments 600 series (SI600s) CCD camera was used. The pixel size of the CCD chip is 15 μm and covers the complete spectral range from around λλ 3650–9400 Å. A total of 27 spectra have been collected for V716 Cen. The journal of the observations is given in Table 1.

For all observations, comparison spectra of a thorium–argon arc lamp are recorded before and after each exposure. The dispersion solution was interpolated between the two thorium spectra for the exact time of the stellar observation, which is a flux-weighted mean obtained from the exposure meter readings during the observation. Exposure time of each stellar spectrum was determined to achieve a desired signal-to-noise ratio (S/N) which was ∼100 around 5500 Å (Table 2). Therefore, once predefined exposure meter reading for S/N ∼ 100 was obtained, the exposure was ended. A set of white lamp images was taken every night for flat-fielding.

All spectra were reduced with the HERCULES Reduction Software Package (HRSP) developed in the department of Physics and Astronomy, University of Canterbury. The procedure of reduction is a standard for échelle spectra (Skuljan 2004).

When normalizing the raw spectra extracted from the CCD images, second- or third-order polynomials were fitted on selected parts of the continuum. The spectra are normalized by division by the fitted polynomials.

3 RADIAL VELOCITIES MEASUREMENTS AND ORBITAL SOLUTIONS

The RV measurements have been performed on the wavelength-calibrated, normalized spectra primarily by line-profile fitting. A

Table 2. Spectral order and stellar lines used in this study, those eligible for RV measurement are marked (X). Unless otherwise stated, only the lines of the primary are available. The rest wavelengths are from the NIST data base. The S/N refers to the continuum.

Order no.	Wavelength region	Line		Mean S/N	Remarks
85	6650–6728	6678.15 (He I)	X	130	Relatively strong
87	6497–6574	6562.85 (Hα)		120	Both component can be seen
89	6351–6426	6371.36 (Si II)	X	120	Weak
97	5828–5896	5875.62 (He I)	X	115	Relatively strong. Badly disturbed by telluric lines of H_2O when shifted to longer wavelength
113	5003–5062	5018.43 (Fe II)	X	90	Relatively weak
		5039.38 (Si II)	X		Weaker than Fe II
127	4452–4504	4471.48 (He I)		90	Relatively strong
		4481.33 (Mg II)	X		Relatively strong, component stars can easily be distinguished
130	4349–4401	4387.93 (He I)	X	85	Relatively weak
		4383.54 (Fe I)			Weaker than He I
131	4316–4367	4340.47 (Hγ)		80	Relatively strong and broad
137	4127–4176	4143.76 (He I)	X	75	Relatively weak
139	4068–4116	4101.74 (Hδ)		75	Relatively strong and broad
141	4009–4058	4026.19 (He I)	X	70	Relatively strong
143	3954–4001	3970.07 (Hϵ)		55	Relatively strong and broad
146	3873–3919	3889.05 (H I)		55	Relatively strong and broad
148	3821–3866	3835.38 (H I)		50	Relatively strong and broad

Downloaded from https://academic.oup.com/mnras/article/385/1/381/1032418 by Akdeniz University user on 20 September 2021

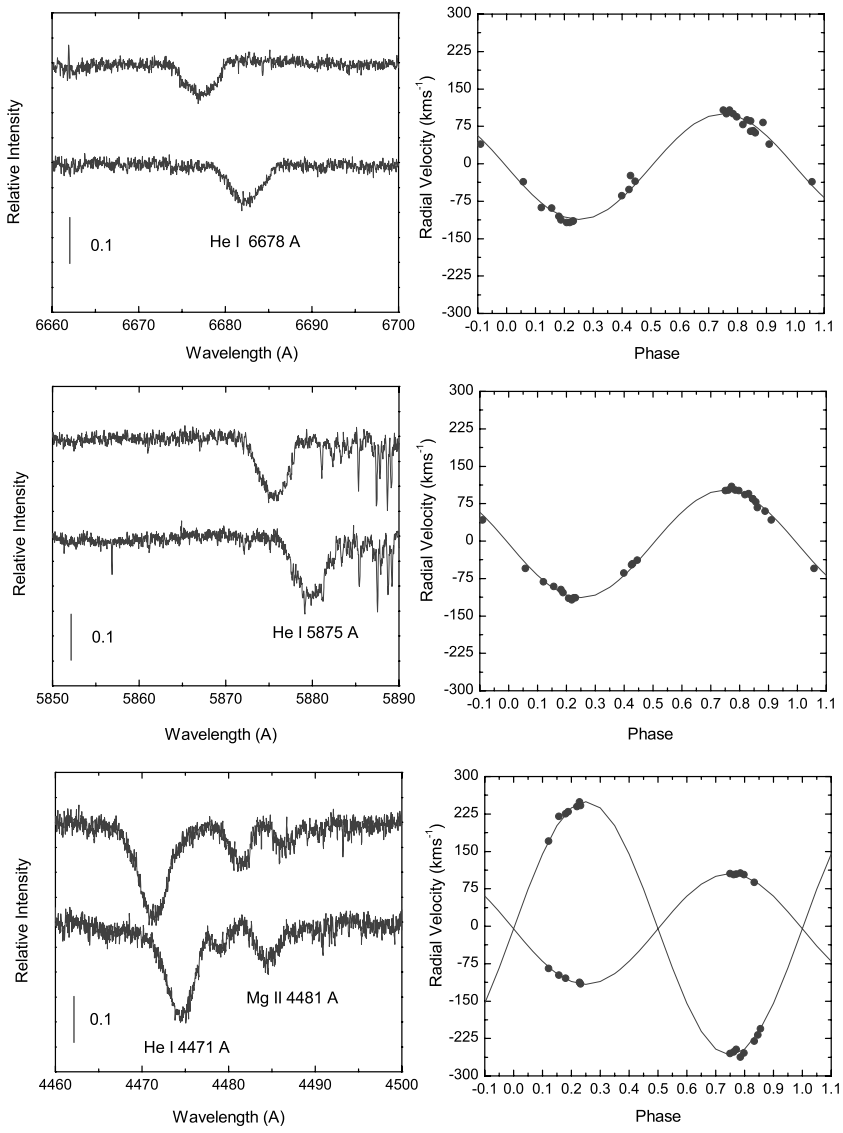


Figure 1. Spectral lines used for RV measurements (panels on the left) and the corresponding orbital fittings (panels on the right). In each panel of the spectral lines, upper spectrum is for orbital phase $\phi \sim 0.25$ and lower spectrum is for orbital phase $\phi \sim 0.75$. Wavelengths are given in vacuum.

method of Fourier disentangling of spectra was also considered as a second method to obtain RVs for comparison. The two independent techniques are useful for inspecting the consistency of RVs and consequently the orbital solutions.

After fitting Gaussian profiles to individual spectral lines using the splot task in IRAF,[1] the Doppler shifts were determined using the rest wavelengths of spectral lines taken from the NIST[2] data base. The échelle orders and lines potentially eligible for measurements are listed in Table 2. Unfortunately, some of these lines are too weak or broad to permit reliable RV measurements therefore they are excluded from our analysis. The lines which were used for line-profile fitting are also given (column 4 of Table 2). The lines of the secondary component are identified with confidence only in two spectral orders, 87 and 127, and due to strong blending of the components the Hα line is useless for RV measurements. It is known that Hα originates not only in the photosphere but may also originate in circumstellar and/or interstellar matter. An investigation of Hα over the orbit is made in Section 5.3. In the spectral order 127, where He I 4471 Å and Mg II 4481 Å are located, only the latter was found in both components. The absorption of the secondary is very weak or absent at He I 4471 Å which indicates a spectral type of A0 or later for the secondary component. Fig. 1 shows selected spectral regions at quadrature and measured RVs with fit models.

Orbital solutions were obtained by the least-squares fitting of theoretical RV curves to the RV measurements of each order independently. The models used the updated light elements of Kreiner, Kim & Nha (2001) and only the velocity amplitudes $K_{1,2}$, systemic velocity V_γ have been converged in the least-squares solution.

The spectra of V716 Cen were also analysed using the new version of the KOREL code, i.e. by the method of Fourier disentangling (Hadrava 1995, 2004), which yields directly the orbital parameters

[1] IRAF is distributed by the National Optical Astronomy Observatories, which is operated by the Association of Universities for Research in Astronomy, Inc. (AURA) under cooperative agreements with the National Science Foundation.
[2] http://www.physics.nist.gov/.

Downloaded from https://academic.oup.com/mnras/article/385/1/381/1032418 by Akdeniz University user on 20 September 2021

Table 3. Spectroscopic orbital parameters of V716 Cen according to KOREL solution.

Parameter	Values
P (d)	1.490 0943
T_0 (HJD)	245 2501.492 ± 0.001
e	0.0
K_1 (km s^{-1})	104.4 ± 0.4
K_2 (km s^{-1})	242.3 ± 0.4
q	0.431 ± 0.003
V_γ (km s^{-1})	−10.3 ± 6.9

and decomposed spectra of the component stars. The KOREL code was applied with the orbital parameters from the line-profile fitting as start values. Spectral lines of both components could be disentangled only from the échelle order 127. Only the lines of primary are reconstructed from the other orders (see Table 2).

In this part of the analysis, the velocities of the centres of light of the stars are assumed to be identical with those of their centres of mass. It is well known that the distorted stellar shapes due to tidal effects and the Rositter–Mc Laughlin effects (eclipse effects) can cause the observed light centres to differ from the mass centres for each component. In principle, both of these effects are important for contact binaries (Hrivnak et al. 1984). The present version of the KOREL code does not allow us to consider the tidal and eclipse effects on the RVs of the components during the orbital solution. By including RVs at eclipse phases (ϕ = 0.057, 0.425, 0.429, 0.445, 0.909), the KOREL solution have differed by as much as five to six times the uncertainties given in Table 3, despite the large common set of data. Clear systematics in the residuals of the radial velocities derived from cross-correlation of the observed with the KOREL component spectra indicate the reduced quality of the orbital solution with all spectra included. Therefore, the spectra taken at eclipse phases were not included in the final KOREL solution.

During the KOREL iteration process only the orbital period P was fixed, so that the conjunction time T_0, eccentricity e, longitude of periastron w and the RV semi-amplitudes K_1 and K_2 were the parameters iterated. The eccentricity did not deviate from zero, so it is kept as zero before obtaining the final set of spectroscopic orbital parameters.

KOREL does not derive the systemic velocity, but it measures the shift of each component relative to the disentangled spectra in which the systemic velocity is retained. Therefore, the systemic velocity V_γ was adopted by averaging systemic velocities obtained from the analysis of spectral orders (Table 2) and measured from the disentangled He I and Mg II lines by means of Gaussian fitting to the centre of these lines. The adopted V_γ velocity (−10.3 ± 6.9 km s^{-1}) was added to the measured RVs by KOREL to yield the final RVs of the components. The estimate from seven different spectral orders shows an rms scatter of 6.9 km s^{-1} around the V_γ velocity.

The parameters from the spectroscopic orbital solution are presented in Table 3 with standard error in each parameter indicated and RVs with their residuals from the orbital solutions are given in Table 4. The errors of parameters are internal. Uncertainties computed with the jackknife method are (up to a factor of 2) higher than these internal errors. The adopted velocity semi-amplitudes K_1 and K_2 listed in Table 3 are those of the light centres of the components and are useful to be used as initial parameters in the combined analysis of the light and RV curves, Section 4, where the tidal and eclipse effects were taken into account to yield the orbital parameters of the mass centres. In Table 4, the RVs at eclipse phases, which were not used with KOREL but are available from the line-profile fitting, are also given for the primary component with their residuals from the theoretical fit. Fig. 2 shows the observed spectra of V716 Cen with the KOREL fits superimposed. The spectra in Fig. 2 are plotted according to the increasing order of phases as listed in Table 4. The disentangled spectral lines for the primary and the secondary are seen below the 27 spectra in the upper panel of Fig. 2.

Table 4. Radial velocities of V716 Cen obtained by the Fourier disentangling of He I 4471 Å and Mg II 4481 Å. The V_γ velocity obtained from the individual disentangled spectral lines of components is added to all velocities.

HJD −240 0000	Phase ϕ	RV$_1$ (km s^{-1})	O − C (km s^{-1})	RV$_2$ (km s^{-1})	O − C (km s^{-1})
539 67.829 64	0.057	−60.3	−13.7	–	–
539 67.923 87	0.120	−81.6	0.0	155.9	−0.1
539 67.977 23	0.156	−96.8	0.0	191.2	0.0
539 76.953 99	0.180	−104.6	0.0	209.4	0.0
539 76.967 30	0.189	−106.9	0.0	214.8	0.0
539 88.915 25	0.207	−110.7	0.0	223.6	0.0
539 91.911 33	0.218	−112.3	0.1	227.4	0.0
539 88.943 53	0.226	−113.3	0.0	229.6	0.0
539 88.951 98	0.232	−113.7	0.1	230.7	0.0
539 69.828 73	0.399	−72.3	−0.1	134.1	−0.1
539 69.867 52	0.425	−58.2	−0.5	–	–
539 66.893 66	0.429	−61.3	−6.1	–	–
539 69.897 77	0.445	−53.1	−7.6	–	–
539 77.802 97	0.750	93.8	−0.7	−252.9	−0.4
539 77.818 95	0.761	93.6	−0.7	−252.3	−0.4
539 77.835 65	0.772	92.8	−0.6	−250.5	−0.4
539 77.853 79	0.784	91.4	−0.6	−247.3	−0.4
539 77.872 76	0.797	89.3	−0.6	−242.4	−0.4
539 77.906 06	0.819	91.9	7.2	−225.2	4.7
539 77.925 81	0.832	80.1	−0.6	−221.0	−0.4
539 77.945 31	0.846	75.6	−0.6	−210.4	−0.4
539 71.986 01	0.846	75.3	−0.6	−209.8	−0.4
539 71.998 55	0.855	72.1	−0.6	−202.2	−0.4
539 89.889 51	0.861	69.4	−0.6	−195.9	−0.4
539 89.906 80	0.873	64.3	−0.6	−184.1	−0.4
539 86.949 14	0.888	57.0	−0.5	−167.2	−0.3
539 95.920 97	0.909	55.4	8.9	–	–

4 SIMULTANEOUS SOLUTIONS OF LIGHT AND RADIAL VELOCITY CURVES

The *Hipparcos* light curve of V716 Cen, which contains 144 data points with an average observational error of $\epsilon \sim 0.007$ mag, was used in the combined analysis of photometric and spectroscopic data.

The Q-method of Johnson & Morgan (1953) has been used to estimate unreddened colours and interstellar reddening. Using the observed colours $U - B = -0.39$ and $B - V = 0.08$ colours from Deutschman et al. (1976), the Q parameter was found to be $Q = -0.448$. The Q-method gave the unreddened colours as $(U - B)_0 = -0.466$ and $(B - V)_0 = -0.149$. Consequently the colour excesses towards V716 Cen are $E(B - V) = 0.229$, $E(U - B) = 0.076$ and the visual extinction is $A_v = 0.710$ mag. Hauck & Mermilliod (1998) gave the intermediate-band $(b - y)$ colour of the system as 0.09. Using $E(B - V)$ from the Q-method in the relation $E(b - y) =$

Downloaded from https://academic.oup.com/mnras/article/385/1/381/1032418 by Akdeniz University user on 20 September 2021

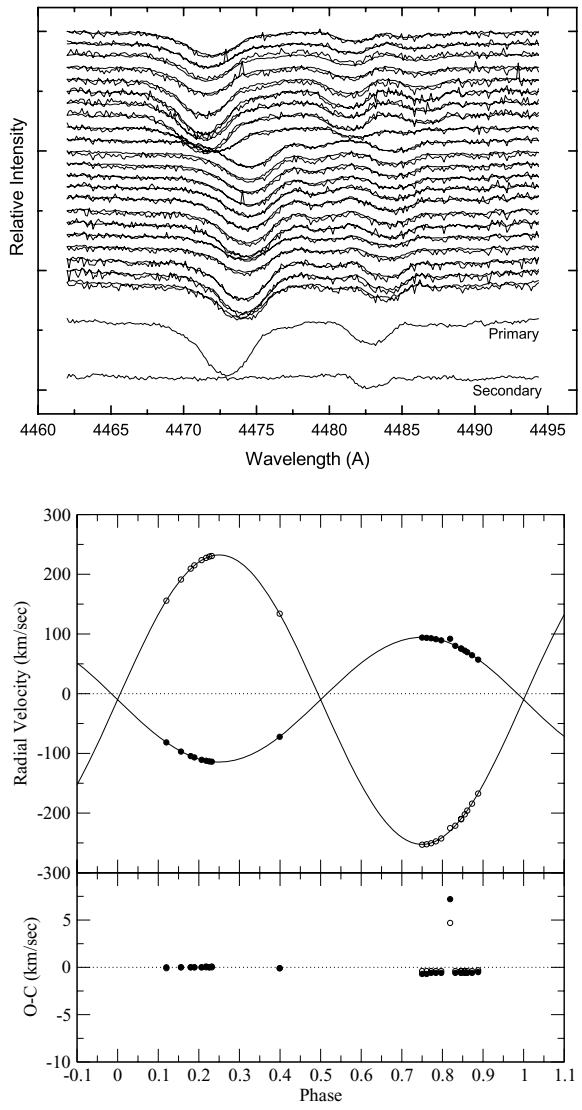


Figure 2. The 27 spectra containing He I λλ4471 Å and Mg II λλ4481 Å lines. Upper panel: Stellar spectra and KOREL fits are superimposed. The disentangled spectra of primary and secondary lines are shown below the observed spectra. Lower panel: Observed and calculated RV curves for V716 Cen. Filled and open circles are our primary and secondary velocities, respectively.

0.70 $E(B-V)$ (c.f. Golay 1974), the colour excess $E(b-y) = 0.16$ corresponding to the unreddened colour of $(b-y)_0 = -0.07$ was deduced. Both $(B-V)_0$ and $(b-y)_0$ are consistent with B5.5V spectral type given in the SIMBAD data base. A temperature of 13 900 K corresponds to the unreddened colour of V716 Cen according to the calibration tables of Budding & Demircan (2007). However, it should be noted that these colours and the corresponding temperature are obtained from the combined light of both component. Since we do not have colour information for eclipse phases, the temperature of the primary must be estimated by another method. This is done in Section 5.2 where the model atmosphere fitting to the primary component's He I 4471 Å and Mg II 4481 Å spectral lines yields a temperature of 15 500 K. Therefore, this temperature was adopted for the temperature of the primary during the light-curve analysis.

Due to the obvious proximity effects in the light curve of V716 Cen, only binary models including a detailed treatment of rotational and tidal distortions can be expected to yield reliable photometric elements. The Wilson–Devinney (WD) (Wilson & Devinney 1971; Wilson 1994) code was chosen for the present analysis. The RVs in partial eclipse which were excluded during the KOREL solution were included this time in the combined analysis. Numerical model parameters are adjusted after a series of test computations based on preliminary elements. The model was applied first to the light and RV curves simultaneously, assuming a detached configuration (Mode 2), but iterations converged quickly to semidetached configuration where the cooler, less massive secondary component fills its critical Roche lobe. Therefore, for the final stage of fitting, the semidetached configuration (Mode 5) was applied.

The temperature of the primary (15 500 K) was fixed during the iterations. The temperature of the secondary component was computed iteratively with the WD program. Gravity darkening exponents $g_1 = g_2 = 1$ were set for radiative envelopes. No third light was assumed. A logarithmic limb-darkening law was used. Bolometric and H_p-band (505-nm) limb-darkening coefficients were taken from van Hamme (1993). Other parameters adjusted were the semimajor axis a, mass ratio q, orbital inclination i, systemic velocity V_γ, potential Ω_1 of the primary and luminosity L_1 of the primary. Ω_2 and L_2 was constrained automatically by the model. Weights for light and RV data were adopted on the basis of uncertainties of the data. For light-curve data, those with catalogue errors less than 0.012 mag were weighted by 10. There are three data points in the light curve with errors equal or bigger than 0.012 mag and these are weighted by 1. An inspection of light-curve plot (Fig. 3) reveals three other data points with small catalogue errors but with unexpected large deviations from the fit. These points have also been treated with low weight although high or low weight of these data has no or very weak influence on the solutions. All the RV data have been treated with high weight since the uncertainty on the RV measurements are similar over all phases.

Bolometric albedos $A_1 = A_2 = 1$ were set for radiative envelopes. However, a value of $A_2 = 0.75$ slightly improved the light-curve fitting. The theoretical result $A = 1.0$, for stars with radiative envelopes, has been discussed in the literature (Rucinski 1970; Napier 1971; Vaz 1985; Vaz & Nordlund 1985; Linnel, Peters & Polidan 1988). Departure of albedos from 1.0 for stars with radiative envelopes is attributed to rapid rotation in early-type stars leading to a layered turbulence (Tassoul & Tassoul 1982), or to helium ionization and radiation pressure rendering OB stars unstable against convection (Underhill & Fahey 1984).

Using WD to fit the radial-velocity curves including the spectra in partial eclipse yields velocity amplitudes that differ by about 30 times the errors of velocity amplitudes given in Table 3. This underlines the fact that the precision on the estimated parameters depends stronger on the level of physics in the code than on the noise in the data (see Section 5.1).

The resulting parameters of the simultaneous solutions of light and RV curves are given in Table 5. Computed light and RV curves fitted to observational data are shown in Fig. 3 together with the equipotential surfaces of the component stars adopted from the model. In the middle panel of Fig. 3 the RVs of the components are shown with two theoretical RV curves. The dashed lines indicate the velocities of the light centres of each component and the solid lines indicate the velocities of the light centres of each component, corrected to include tidal and eclipse effects.

Downloaded from https://academic.oup.com/mnras/article/385/1/381/1032418 by Akdeniz University user on 20 September 2021

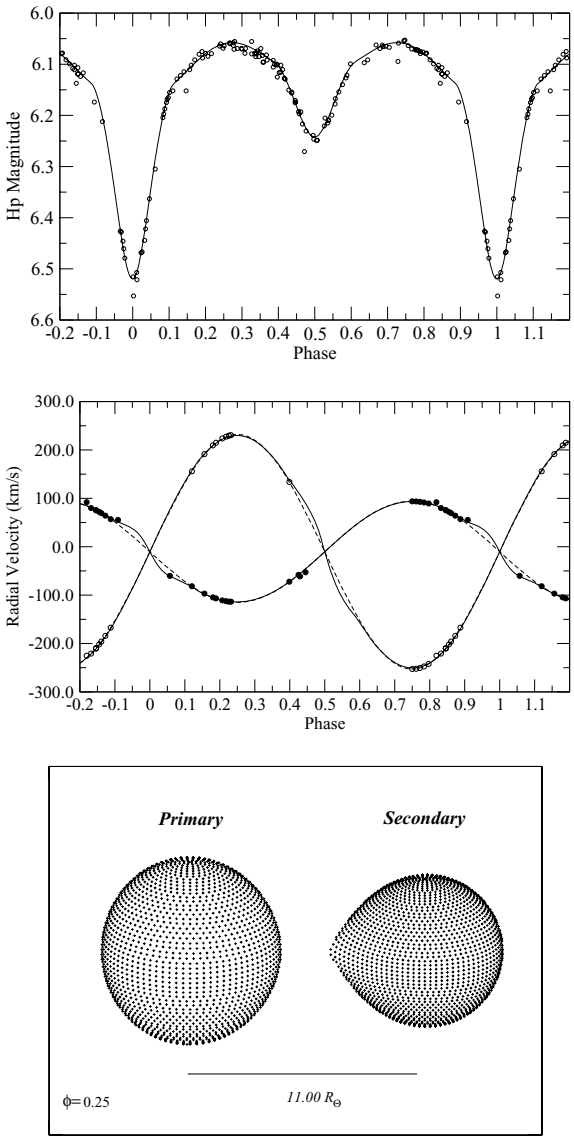


Figure 3. The light (top panel) and RV (middle panel) curves fitted to the observed data of the V716 Cen system. The equipotential surfaces of the stars according to the adopted model are shown in the bottom panel.

5 DISCUSSION

5.1 The close binary stellar parameters

The use of a physical model of the system based upon the light and RV curve analysis has enabled us to obtain the mass ratio and the velocity semi-amplitudes of the mass centres. The physical model also allows us to investigate the tidal and eclipse effect. The eclipse effects occur in the velocity curve of the component being eclipsed due to the net rotation of the uneclipsed portion of the star. This effect shows itself for the primary component in the phase ranges 0.01–0.12 and 0.88–0.99, and for the secondary component in the phase ranges 0.39–0.50 and 0.50–0.61. At $\phi = 0.04$ the correction to the velocity curve of the primary component is -19 km s^{-1}, and at $\phi = 0.54$ the correction to the velocity curve of the secondary component is -32 km s^{-1}. As almost all the RV data in our analysis come from the observations nearer to quadratures, few spectra are influenced.

Table 5. Simultaneous light and RV solution for V716 Cen. The parameters without errors are coupled to the other parameters or fixed.

Parameter	Primary	Secondary
V_γ (km s^{-1})	-10.3 ± 6.9	
a(R$_\odot$)	11.00 ± 0.03	
i(°)	71.9 ± 0.2	
e	0.0	
$T_{1,2}$ (K)	15 500	9000 ± 80
$\Omega_{1,2}$	3.183 ± 0.038	2.728
$q(M_2/M_1)$	0.420 ± 0.003	
$L_{1,2}(L_{1,2}/L_{\rm Total})$	0.823 ± 0.004	0.177 ± 0.004
$r_{1,2}$(pole)	0.359 ± 0.005	0.287 ± 0.001
$r_{1,2}$(point)	0.393 ± 0.007	0.413 ± 0.001
$r_{1,2}$(side)	0.372 ± 0.006	0.299 ± 0.001
$r_{1,2}$(back)	0.383 ± 0.006	0.332 ± 0.001
$r_{1,2}$(mean)	0.371 ± 0.006	0.306 ± 0.001
$A_{1,2}$	1.000	0.750 ± 0.050
$g_{1,2}$	1.0	
$F_{1,2}$	1.0	

The tidal effects cause the projected light centres to differ from the projected mass centres. Since it is essentially the motion of the light centres which we are measuring, this can effect our values of K_1 and K_2, thus q. The correction for this is most pronounced at the quadratures of the velocity curves. At $\phi = 0.25$ this correction amounts to 1 km s^{-1} for the primary component, and 10 km s^{-1} for the secondary component. The bigger correction in the velocity semi-amplitude of the secondary is clearly the consequence of the distorted shape of the secondary, the Roche lobe filling star. As a consequence of the impact on the velocity semi-amplitudes, neglect of this tidal effect would lead to underestimation of the masses by about 8 and 5 per cent for the primary and secondary components, respectively.

The physical dimensions of V716 Cen which were derived from the results in Table 5 are summarized in Table 6. Using the inclination of 71°.9 found from the combined analysis of photometric and spectroscopic data, we arrive at the following masses for the components: $M_1 = 5.68\,{\rm M}_\odot$ and $M_2 = 2.39\,{\rm M}_\odot$. The separation between the components is $a = 11.00\,{\rm R}_\odot$. The masses are consistent with spectral types of B5V and A2V for the primary and the secondary components, respectively.

Table 6. The astrophysical parameters of V716 Cen according to the results of WD solution given in Table 5.

Parameter	Primary	Secondary
P (d)	1.490 0943 ± 0.000 0004	
T_0 (HJD)	245 2501.492 ± 0.003	
M(M$_\odot$)	5.68 ± 0.07	2.39 ± 0.05
R(R$_\odot$)	4.08 ± 0.07	3.36 ± 0.02
$T(K)$	$15\,500 \pm 50$	9000 ± 80
log L(L$_\odot$)	2.93 ± 0.03	1.82 ± 0.02
a(R$_\odot$)	11.00 ± 0.03	
log g (CGS)	3.970 ± 0.010	3.762 ± 0.012
$V_{\rm sync}$ (km s^{-1})	139 ± 3	115 ± 2
$V_{\rm obs}$ (km s^{-1})	137 ± 2	116 ± 7
M$_{bol}$ (mag)	-2.59 ± 0.07	0.19 ± 0.05
BC	-1.20	-0.14
M_v (mag)	-1.39 ± 0.07	0.33 ± 0.05
d (pc)	339 ± 8	

Downloaded from https://academic.oup.com/mnras/article/385/1/381/1032418 by Akdeniz University user on 20 September 2021

Table 7. Rotational standard stars selected from the compilation of Slettebak et al. (1975).

Star	$v \sin i$ (km s^{-1})	FWHM (Å)
HD47306	40	0.953
HD29875	40	1.301
HD181869	70	1.501
HD16978	90	2.037
HD198001	85	2.084
HD12311	120	3.046
HD15008	155	3.343
HD148605	180	3.838
HD2262	225	4.279
HD209952	215	5.344

Bolometric corrections of the components were taken from the table of empirical calibrations for main-sequence stars by Budding & Demircan (2007). Absolute luminosities L_1, L_2 and the distance modulus, which uses the absolute bolometric magnitudes in Table 6, indicate a photometric distance of 339 ± 8 pc for the V716 Cen system. The less accurate *Hipparcos* parallax (2.96 ± 0.63 mas) gives a distance of 337 ± 72 pc in agreement with the photometric distance.

5.2 Rotational velocities and synchronization

Determination of rotational velocities was performed using two independent techniques. First, we have observed 10 rotational velocity standard stars taken from the compilation of Slettebak et al. (1975). Full width at half-maximum (FWHM) measurements of the Mg II 4481 Å lines in the spectra of these stars were made by fitting a Gaussian profile to the Mg II lines using the splot task implemented in IRAF. The measured FWHM values of the Mg II lines of the standard stars were compared to their catalogue velocities (Table 7). For the spectra obtained at MJUO, a linear least-squares fitting to the measurements yields the calibration equation as

$$(v_{\rm rot} \sin i) = 46(\pm 4) \times {\rm FWHM7}(\pm 12). \quad (1)$$

Fig. 4 shows the observed standard stars with their names and the corresponding best linear fit. Using equation (1) and the inclination of 71°.9, the measured FWHM of the Gaussian fit to the Mg II lines, 2.92 and 2.63 Å for primary and secondary respectively, yield rough

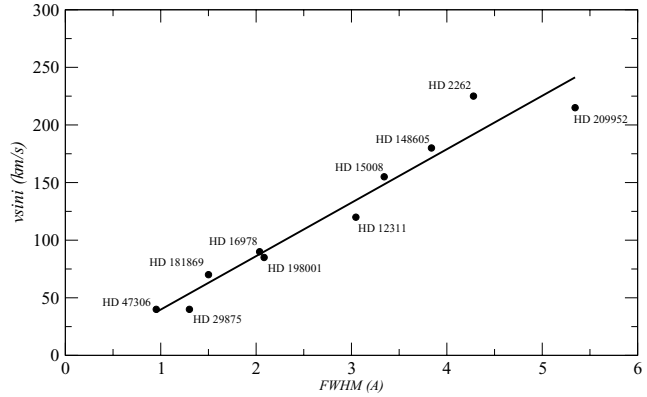


Figure 4. FWHM–($v_{\rm rot} \sin i$) calibration for 10 standard stars of Slettebak et al. (1992).

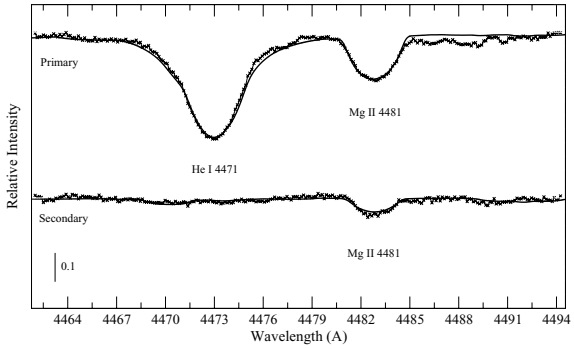


Figure 5. Model atmosphere line profiles (continuous lines) compared to the disentangled (plus signs) He I 4471 Å and Mg II 4481 Å lines of the primary component (top) and Mg II 4481 Å line of the secondary component (bottom).

estimates of rotational velocities as $(v_{\rm rot})_1 = 143 \pm 20$ km s^{-1} and $(v_{\rm rot})_2 = 127 \pm 20$ km s^{-1}.

Secondly, we have calculated model atmospheres and synthetic spectra of components for comparison with their observed spectra. This method yields atmosphere parameters as well as more precise rotational velocities of component stars. Assuming solar metallicity ([M/H] = 0.0 dex) and microturbulent velocity (ζ) of 2 km s^{-1}, a grid of atmosphere models was calculated using the ATLAS9 code (Kurucz 1993) and the synthetic spectra were produced for the primary and secondary components using the SYNTHE code (Kurucz 1993) under Linux. To set the model parameters, we proceeded by iterations on the basis of $\chi^2_{\rm min}$ minimization, starting with colour temperatures ($T_{\rm eff1,2}$) and surface gravities ($\log g_{1,2}$) from light- and velocity-curve analysis section (Section 4). The surface gravities ($\log g_{1,2}$) were fixed at the values obtained from the light-curve solution, therefore temperatures ($T_{\rm eff1,2}$) and the projected rotational velocities [$(v_{\rm rot})_{1,2}$] of the components were the parameters adjusted. The renormalization of the synthetic lines was performed in a standard way (i.e. Bakış, Eker & Demircan 2007) which takes into account the light contributions of the components. In Section 4, the light-curve analysis yielded the components' light ratio in the $H_{\rm p}$ band (505 nm) as 82 and 18 per cent, and similar light contribution have been obtained from the fitting of synthetic spectra to the observed spectra in échelle order 127. Our best-fitting atmosphere models yield the light contributions for the components as 87 and 13 per cent at 448 nm wavelength. The resultant atmosphere parameters and rotational velocities of stars were obtained as $T_{\rm eff1} = 15\,500 \pm 50$ K, $T_{\rm eff2} = 9500 \pm 300$ K, $(v_{\rm rot} \sin i)_1 = 130 \pm 2$ km s^{-1}, $(v_{\rm rot} \sin i)_2 = 110 \pm 3$ km s^{-1}. With the inclination of 71°.9, $(v_{\rm rot})_1 = 137 \pm 2$ km s^{-1} and $(v_{\rm rot})_2 = 116 \pm 5$ km s^{-1}. The resulting synthetic lines are shown in Fig. 5.

Due to their more precise values, the equatorial rotational velocities are adopted from model atmosphere fitting as $(v_{\rm rot})_1 = 137 \pm 2$ and $(v_{\rm rot})_2 = 116 \pm 5$ which are in close agreement with the synchronous rotation velocities [$(v_{\rm sync})_1 = 139 \pm 3$ km s^{-1} and $(v_{\rm sync})_2 = 115 \pm 2$ km s^{-1}] of components. Thus, the validity of the synchronous rotation for both components is clear within the errors limits.

5.3 Circumstellar matter

An effective way of investigating the circumstellar matter around interacting binary stars is to study the variations and/or emission structures of Hα in the stellar spectra (cf. Albright & Richards

Downloaded from https://academic.oup.com/mnras/article/385/1/381/1032418 by Akdeniz University user on 20 September 2021

1995; Koubskỳ, Richards & Šimon 1998; Richards & Albright 1999; Harmanec et al. 2002; Saad et al. 2004). Therefore, 25 high-resolution ($\lambda/\delta\lambda = 41\,000$) H$\alpha$ line profiles were studied in the present paper. In order to investigate the emission structure, difference profiles were produced. Two methods are especially effective to obtain difference profiles. (i) By calculating synthetic lines using model atmospheres based on the adopted system parameters (temperature, surface gravity and rotational velocity), applying orbital motion to the synthetic spectra and convolving the individual synthetic spectra of component stars using the light ratios in the studied wavelength region. Finally, the difference profiles can be obtained by subtracting this synthetic spectrum from the observed ones. (ii) By using the KOREL code to reconstruct the component spectra and subtract them from the observed ones with the correct Doppler shifts and light dilution factors. Method (ii) is adequate in our case since the dilution factor in the Hα region is not known a priori.

The Hα line profile in our spectra is close to the edge of the order of 87 and thus, there are edge effects. In order to get rid of the systematic effects in the difference profiles, normalization of the spectra was performed by fitting same function to the same selected sample regions in the spectra. The same process is applied for the spectral order 86 which represents a small part of the longer wavelength Hα wing.

The orbital parameters derived in Table 3 were fixed during the disentangling of spectra. Spectral line strengths of components were fixed for the spectra at out-of-eclipse phases while they were allowed to converge only for the eclipsed component during the eclipses. Once the spectral lines of components have been disentangled from the composite spectrum, difference profiles were constructed by subtracting the average spectrum from the observed spectra. Fig. 6 shows the observed Hα line profiles superimposed with KOREL fits and disentangled profiles of component stars. During the decomposition of spectra, the telluric lines were also taken into account. Disentangled telluric lines are displayed in Fig. 6.

The three-component disentangling is not fully successful in the sense that at least the low-frequency components of the telluric spectrum and the secondary component are ill determined (Fig. 6). For our purpose, this is not of prime importance since the influence on the combined-component spectra subtracted from the observed spectra is small, as the bias in the telluric spectrum and that of the secondary component are opposite and therefore cancel to a large extent.

In the lower panel of Fig. 6, difference profiles were shown with the corresponding orbital phases indicated, where we see that there is no significant deviation of O − C residuals from zero. The only deviations from zero are due to poor telluric line correction during the decomposition of spectra. Therefore, it seems fair to conclude that there is no clear-cut observational evidence for significant amounts of circumstellar matter in the system and, in fact, the configuration for the system we have found in Section 4 would leave little space to store such gas permanently around the primary star.

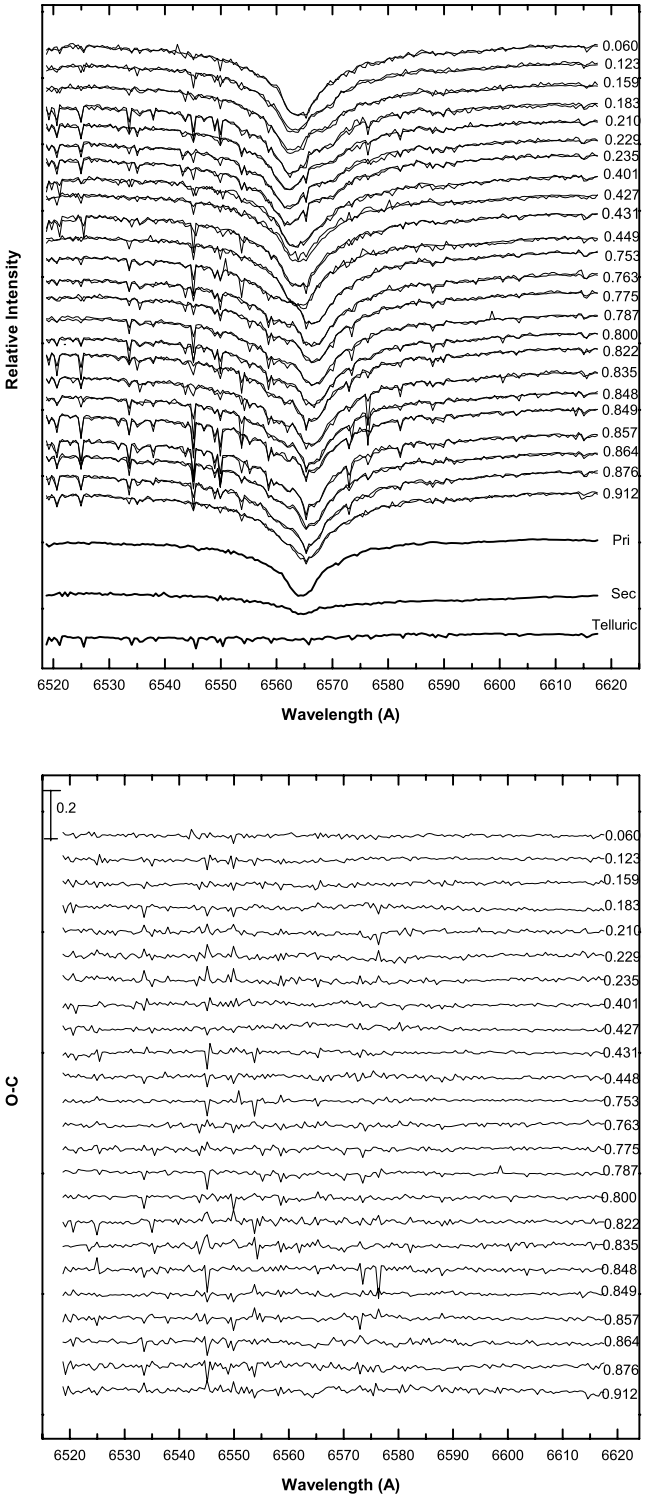


Figure 6. KOREL fits to the composite Hα spectral lines of V716 Cen. The disentangled spectra of the primary and secondary component and the disentangled telluric line spectrum are shown in the lower part of the upper panel. In the lower panel, the difference profiles of the observed spectra with the KOREL fits are plotted. The orbital phases are displayed near each difference profile.

5.4 Evolutionary status

The location of the component stars in temperature–luminosity, temperature–gravity and mass–radius planes are displayed in Fig. 7. In each panel of Fig. 7, the zero-age main-sequence (ZAMS) and terminal-age main-sequence (TAMS) of Girardi et al. (2000) are plotted. A literature search reveals that the OB-type binaries such as TT Aur (Özdemir et al. 2001), SX Aur (Chambliss & Leung 1979), XZ Cep, V448 Cyg (Harries, Hilditch & Hill 1997), U Her

Downloaded from https://academic.oup.com/mnras/article/385/1/381/1032418 by Akdeniz University user on 20 September 2021

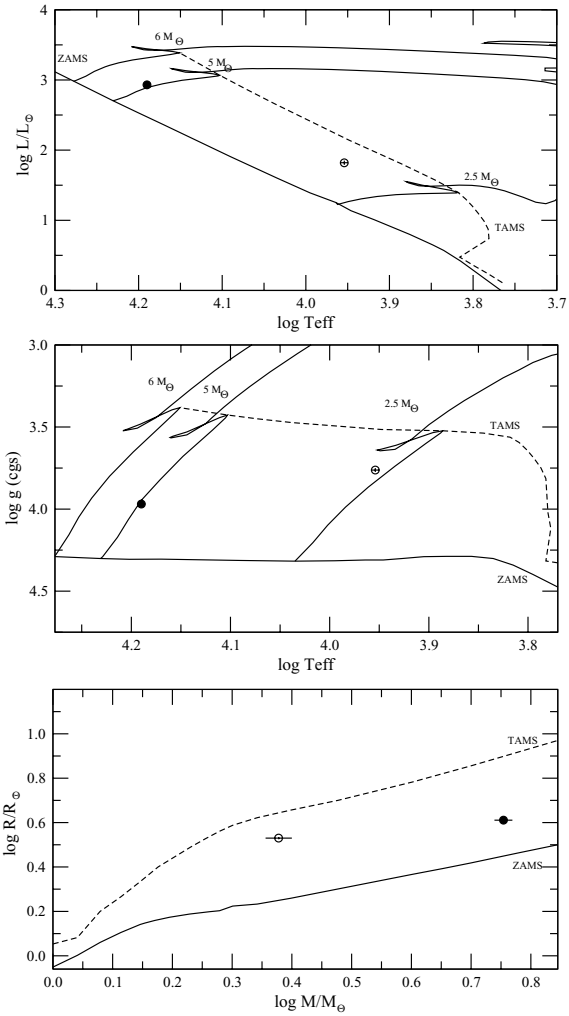


Figure 7. Temperature–luminosity (upper panel), temperature–gravity (middle panel) and mass–radius (lower panel) relations depicting the location of the components of V716 Cen with respect to the ZAMS and the TAMS.

(Hilditch 1984), VY Lac (Semeniuk & Kaluzny 1984), β Lyr (Harmanec 1990), DM Per (Hilditch, Hill & Khalesseh 1992), IZ Per (Srivastava & Padalia 1970), V356 Sgr, Z Vul (Hilditch & Bell 1987), V Pup (Andersen et al. 1983), μ^1 Sco (Schneider, Darland & Leung 1979), V337 Aql (Giuricin & Mardirossian 1981), IU Aur (Giuricin et al. 1979) and LY Aur (Cester et al. 1978) are all similar to V716 Cen. All of these systems are semidetached and mass transfer occurs from the less massive, Roche lobe filling secondary component to the more massive primary in core hydrogen-burning phase, namely Case A (Paczyński 1971). Although the total mass of V716 Cen is less than in most of these OB-type systems, the similarities between V716 Cen and these systems on the basis of early spectral types of component stars, Case A type mass exchange between components, mass transfer from the less massive secondary to the primary and the location of component stars in Hertzsprung–Russell (HR) diagrams are very striking and it can be concluded that V716 Cen has evolved through a phase of rapid mass exchange and mass-loss. The originally more massive component is now the less massive one. The mass gaining component is not able to assimilate the additional mass immediately and shows up in the HR diagram as a star underluminous for its mass. This case was investigated recently by İbanoğlu et al. (2006) who compared the primaries of semidetached binary systems to the primaries of the same mass in detached binary systems. Their study showed clear evidence for the primaries in semidetached systems being less luminous than the primaries of the same mass in detached systems. On the contrary to the scenario drawn above for the primary, the mass-losing secondary component becomes overluminous after the rapid mass exchange. The present location of the components in the HR diagram (Fig. 7) seems to support the suggested evolutionary scenario for the V716 Cen system. It is expected that the secondary component of V716 Cen will continue to transfer mass to its companion until the mass ratio of the system would decrease to very low values, may be near the lower limit of the mass ratio of classical Algols.

ACKNOWLEDGMENTS

This study is the part of a project carried out in Southern hemisphere which is supported by The Scientific & Technological Research Council of Turkey (TUBITAK) under the project code 2214 and partly by Çanakkale Onsekiz Mart University Research Foundation. It is also part of the PhD thesis of HB who would like to thank Professor John Hearnshaw for granting observing time, Professor Ed Budding for the discussions during the preparation of the project, Carter Observatory Board for providing an office and technical staff (Alan Gilmore, Pam Kilmartin, Steven Barlow, Nigel Frost and Paul Tristram) at MJUO and for their warm hospitality during her research programme in New Zealand, and members of the Physics and Astronomy Department at the University of Canterbury for their warm hospitality. HB would also like to thank Dr Hasan Ak for his valuable comments and discussions. We like to express a sincere gratitude to the reviewer, Herman Hensberge, that his useful comments improved the quality of the presentation of this paper.

REFERENCES

Albright G. E., Richards M. T., 1995, Ap&SS, 224, 415
Andersen J., Clausen J. V., Gimenez A., Nordstroem B., 1983, A&A, 128, 17
Bakış H., Eker Z., Demircan O., 2007, MNRAS, 382, 609
Bekenstein J. D., Bowers R. I., 1974, ApJ, 190, 653
Budding E., Demircan O., 2007, Introduction to Astronomical Photometry, 2nd edn. Cambridge Univ. Press, Cambridge
Cester B., Fedel B., Giuricin G., Mardirossian F., Mezzetti M., 1978, A&A, 62, 291
Chambliss C. R., 1969, IBVS, 408
Chambliss C. R., Leung K. C., 1979, ApJ, 228, 828
Cousins A. W. J., Stoy R. H., 1962, R. Obs. Bull., 64, 103
Deutschman W. A., Davis R. J., Schild R. E., 1976, ApJS, 30, 97
ESA, 1997, The *Hipparcos* Catalogue, ESA SP-1200
Fitzgerald M. P., 1970, A&A, 4, 234
Girardi L., Bressan A., Bertelli G., Chiosi C., 2000, A&AS, 141, 371
Giuricin G., Mardirossian F., 1981, A&AS, 45, 499
Giuricin G., Mardirossian F., Mezzetti M., Cester B., 1979, A&AS, 37, 513
Golay M., 1974, Introduction to Astronomical Photometry. Reidel, Dordrecht
Hadrava P., 1995, A&AS, 114, 393
Hadrava P., 2004, Publ. Astron. Inst. Cz., 92, 15
Harries T. J., Hilditch R. W., Hill G., 1997, MNRAS, 285, 277
Harmanec P., 1990, A&A, 237, 91
Harmanec P., 2001, Publ. Astron. Inst. Cz., 89, 9
Harmanec P., Bisikalo D. V., Boyarchuk A. A., Kuznetsov O. A., 2002, A&A, 396, 937
Hauck B., Mermilliod M., 1998, A&AS, 129, 431

Downloaded from https://academic.oup.com/mnras/article/385/1/381/1032418 by Akdeniz University user on 20 September 2021

Hearnshaw J. B., Barnes S. I., Kershaw G. M., Frost N., Graham G., Ritchie R., Nanakivell G. R., 2002, Exp. Astron., 13, 59
Hilditch R. W., 1984, MNRAS, 211, 943
Hilditch R. W., Bell S. A., 1987, MNRAS, 229, 529
Hilditch R. W., Hill G., Khalesseh B., 1992, MNRAS, 254, 82
Hoogerwerf R., de Bruijne J. H. J., de Zeeuw P. T., 2001, A&A, 365, 49
Hrivnak B. J., Milone E. F., Hill G., Fisher W. A., 1984, AJ, 285, 683
Hube D. P., 1970, Mem. R. Astron. Soc., 72, 233
İbanoğlu C., Soydugan F., Soydugan E., Dervişoğlu A., 2006, MNRAS, 373, 435
Johnson H. L., Morgan W. W., 1953, ApJ, 117, 313
Johnson H. L., Iriarte B., Mitchell R. I., Wisniewskj W. Z., 1966, Commun. Lunar Planet. Lab., 4, 99
Koubskỳ P., Richards M. T., Šimon V., 1998, in Dušek J., Zejda M., eds, Proc. 20th Stellar Conference of the Czech and Slovak Astronomical Institutes. Nicholas Copernicus Observatory, Brnl, p. 64
Kreiner J. M., Kim C. H., Nha I. S., 2001, An Atlas of OC Diagrams of Eclipsing Binary Stars. Wydawnictwo Naukowe Akademii Pedagogicznej, Krakow
Kurucz R. L., 1993, CD-ROM 13, 18, http://kurucz.harward.edu
Linnel A. P., Peters G. J., Polidan R. S., 1988, ApJ, 327, 265
Napier W. Mcd., 1971, Ap&SS, 11, 475
Özdemir S., Ak H., Tanriver M., Gülseçen H., Gülseçen S., Saygaç A. T., Budding E., Demircan O., 2001, PASA, 18, 152
Paczyński B., 1971, ARA&A, 9, 183
Popper D. M., 1966, AJ, 71, 175
Richards M. T., Albright G. E., 1999, ApJS, 123, 537
Rucinski S. M., 1970, Acta Astron., 20, 327
Saad S. M. et al., 2004, A&A, 419, 607
Sahade J., 1952, ApJ, 116, 27
Schöffel E., Köhler U., 1965, IBVS, 77
Schneider D. P., Darland J. J., Leung K. C., 1979, AJ, 84, 236
Semeniuk I., Kaluzny J., 1984, Acta Astron., 34, 207
Skuljan J., 2004, in Kurtz D. W., Pollard K. R., eds, ASP Conf. Ser. Vol. 310, Variable Stars in the Local Group. Astron. Soc. Pac., San Francisco, p. 575
Skuljan J., Ramm D. J., Hearnshaw J. B., 2004, MNRAS, 352, 975
Slettebak A., Collins G. W. II, Parkinson T. D., Boyce P. B., White N. M., 1975, ApJS, 29, 137
Srivastava R. K., Padalia T. D., 1970, Bull. Astron. Inst. Czech., 21, 359
Tassoul J. L., Tassoul M., 1982, ApJ, 261, 265
Underhill A. B., Fahey R. P., 1984, ApJ, 280, 712
van Hamme W., 1993, AJ, 106, 2096
Vaz L. P. R., 1985, Ap&SS, 113, 349
Vaz L. P. R., Nordlund A., 1985, A&A, 147, 281
Wesselius P. R., 1981, IBVS, 2044
Wesselius P. R., van Duinen R. J., Aalders J. W. G., Kester D., 1980, A&A, 85, 221
Wilson R. E., 1994, PASP, 106, 921
Wilson R. E., Devinney E. J., 1971, ApJ, 166, 605

This paper has been typeset from a TEX/LATEX file prepared by the author.

Downloaded from https://academic.oup.com/mnras/article/385/1/381/1032418 by Akdeniz University user on 20 September 2021